Spin-$\frac{1}{2}$ chain compound $Ba_2Cu_2Te_2P_2O_{13}$: Magnetization, specific heat, and local-probe NMR

Vinod Kumar [1,*] Aga Shahee [1,2] S. Kundu [1] M. Baenitz,[3] and A. V. Mahajan [1,†]

[1]*Department of Physics, Indian Institute of Technology Bombay, Mumbai 400076, India*

[2]*Center for Novel States of Complex Materials Research, Department of Physics and Astronomy, Seoul National University, Seoul 151-747, Republic of Korea*

[3]*Max Planck Institut für Chemische Physik fester Stoffe, Nöthnitzer Strasse 40, 01187 Dresden, Germany*

(Received 21 May 2020; accepted 17 August 2020; published 15 September 2020)

We present synthesis and characterization of $Ba_2Cu_2Te_2P_2O_{13}$ (BCTPO) via x-ray diffraction, magnetic susceptibility, heat capacity, and ^{31}P nuclear magnetic resonance (NMR) measurements. BCTPO crystallizes in a monoclinic structure with Cu^{2+} ions forming coupled chains. In magnetization $M(T)$ measurements, a broad maximum is observed around 53 K. Upon the application of magnetic fields, a sharp anomaly evolves around 4 K in the heat capacity $C_P(T)$ data, indicative of long-range order, while it is absent in zero field. The ^{31}P NMR line shift at about 93.954 kOe tracks the spin susceptibility, whereas the line broadening evidences the onset of magnetic order at about 4 K or lower. The inferred isotropic and axial components of the hyperfine coupling constant are $A_{hf}^{iso} \simeq 3635$ Oe/μ_B and $A_{hf}^{ax} \simeq 479$ Oe/μ_B, respectively. The ^{31}P NMR spin-lattice relaxation rate $1/T_1$ shows a pronounced divergence for $T \longrightarrow 0$. We assign this behavior to critical fluctuations on the verge of order.

DOI: 10.1103/PhysRevB.102.104419

I. INTRODUCTION

Since the early 1970s, there has been a lot of interest in the magnetic properties of low-dimensional Heisenberg antiferromagnetic (HAF) spin systems as they exhibit rich physics and are amenable to comparison with theoretical expectations [1,2]. The primary curiosity here is the intrinsic strong quantum fluctuations which lead to the destruction of long-range magnetic ordering [3]. One-dimensional (1D) magnetic systems have further attracted considerable theoretical attention for the possibility to calculate exactly the ground state energy, excitation spectra, and thermodynamic quantities in a few of these 1D magnetic materials. Since the pioneering work by Bethe [4], it has been known that there are qualitative differences between integer spin and half-integer spin HAF chains. The integer spin HAF chains are gapped, and half-integer spin chains are gapless and show quasi-long-range magnetic order. In the case of an $S = \frac{1}{2}$ AFM Heisenberg chain with comparable next-nearest neighbor AFM exchange, a gap opens up and exhibit novel properties arise from quantum effects. These include the low-temperature rapid decrease in magnetic susceptibility in an $S = \frac{1}{2}$ Heisenberg antiferromagnet [5,6], the dimerized state in the $S = \frac{1}{2}$ quasi 1D magnet [7,8], the disorder-induced long-range ordering in the spin-Peierls system [9,10], and the magnetic and superconducting properties of $S = \frac{1}{2}$ spin ladder [11].

The $S = \frac{1}{2}$ system containing Cu^{2+} ions have drawn particular interest mainly due to high ordering temperatures, large exchange interactions, high quantum fluctuations, multiferroic properties etc. Many $S = \frac{1}{2}$ chain systems have been reported to harbor exciting physics [12]. In the family of $S = \frac{1}{2}$ systems, we came across a new tellurophosphate compound $Ba_2Cu_2Te_2P_2O_{13}$ (BCTPO) which is composed of chains of square planar CuO_4 units connected by PO_4 tetrahedra and trigonal bipyramidal TeO_4 units, and which might behave as a 1D HAF system [13].

In an earlier work on BCTPO, magnetization and heat capacity were reported (up to 10 kOe) and no evidence of long-range magnetic order (LRO) was found down to 2 K. We have synthesized single phase, polycrystalline samples of BCTPO and have investigated its properties in great detail via field dependent magnetization, heat capacity, and local probe technique ^{31}P NMR. While a broad maximum is observed in the susceptibility around 53 K, a clear anomaly is seen in the heat capacity at $T \sim 4$ K on the application of magnetic field larger than 30 kOe, which is likely a sign of long-range magnetic order. The local probe ^{31}P NMR supports this conclusion.

II. EXPERIMENTAL DETAILS

BCTPO was prepared by conventional solid-state reaction methods. Stoichiometric amounts of $BaCO_3$ (Alfa Aesar 99.95%), TeO_2 (Alfa Aesar 99.99%), CuO (Alfa Aesar 99.995%), and $NH_4H_2PO_4$ (Loba Chemie) were taken and ground thoroughly. The mixture was calcined at 700 °C with some intermediate grindings. The room temperature powder x-ray diffraction (XRD) was performed with a PANalytical X'pertPRO diffractometer having a Cu target with $K\alpha$ radiation ($\lambda = 1.54182$ Å). Magnetization measurements were performed in the temperature range 2–400 K with applied

*vinodkiitb@gmail.com
†mahajan@phy.iitb.ac.in

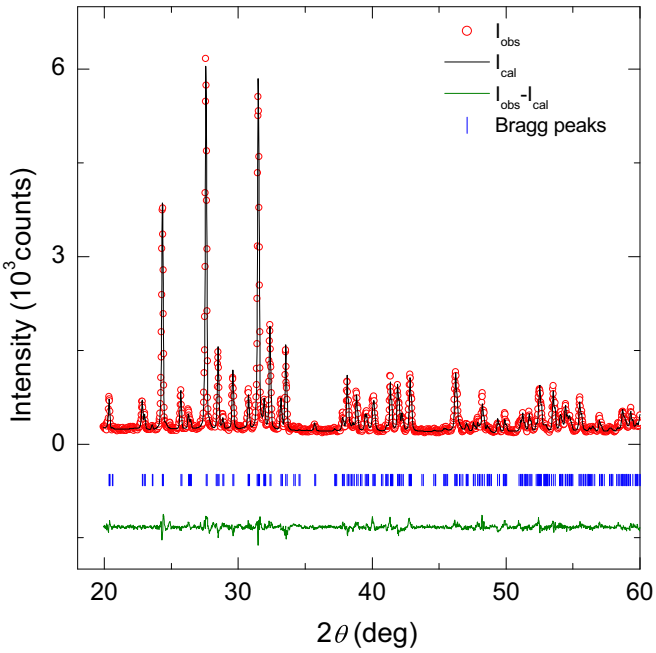

FIG. 1. XRD pattern of $Ba_2Cu_2Te_2P_2O_{13}$ measured at 300 K with a wavelength of 1.54182 Å. The red circles are experimental data, and the solid black line is the theoretically calculated fit by Rietveld analysis. The solid green line is the difference between the experimental and theoretically calculated patterns. The vertical blue bars are the expected Bragg positions for BCTPO.

field values in the range 0–70 kOe using a Quantum Design superconducting quantum interference device vibrating sample magnetometer. Specific heat measurements were carried out in the temperature range 2–300 K and magnetic field range 0–90 kOe using the heat capacity option of a Quantum Design physical property measurement system. The ^{31}P NMR measurements were performed using pulsed NMR techniques in a fixed magnetic field of 93.954 kOe with a Tecmag spectrometer, and the temperature was varied from 4 to 300 K with an Oxford continuous-flow cryostat.

III. RESULTS

A. XRD refinement and crystal structure

The XRD pattern for BCTPO is shown in Fig. 1. To check its phase purity and to refine the atomic positions and lattice parameters, we performed Rietveld refinement of the XRD pattern using the FULLPROF suite [14]. The refinement parameters and the cell parameters are shown in Table I. After refinement the obtained cell parameters are $a = 17.6634(2)$ Å, $b = 7.2850(1)$ Å, and $c = 9.2103(1)$ Å, with $\alpha = \gamma = 90^\circ$ and $\beta = 100.029(1)^\circ$, and the atomic positions are shown in Table II and are in good agreement with Ref. [13]. BCTPO crystallizes in a monoclinic structure with space group $C12/c1$ (space group No. 15). The unit cell of BCTPO is shown in Fig. 2(a). It has the two-dimensional layered structure shown in Fig. 2(b), in which Cu-Cu intrachain interaction takes place via the paths Cu-O-P-O-Cu and Cu-O-Te-O-Cu in the *a*-*c* plane. Also, the interchain magnetic interaction possibly takes place in the *a*-*c* plane via the path Cu-O-Te-O-Te-O-Cu, which is shown in Fig. 2(c). In Fig. 2(d) interlayer interaction among Cu^{2+} ions is shown with exchange coupling J_3 via the path Cu-O-Te-O-P-O-Cu. In BCTPO the Cu-O-(P/Te)-O-Cu path exchange likely leads to a stronger Cu-Cu interaction compared to the Cu-O-Te-O-Te-O-Cu path due to the presence of an extra Te bipyramid in the latter. Therefore, we expect a magnet with coupled chains, intrachain coupling J_1 and interchain couplings J_2 and J_3 [$(J_3 < J_2) < J_1$], as illustrated in Fig. 2. The distribution of Cu^{2+} ions around P is shown in Fig. 2(e). P is surrounded by three Cu^{2+} ions with P at its center. Among the three Cu^{2+} ions, two occupy the same Wyckoff position with bond lengths of 3.28(1) and 3.82(1) Å, whereas the third Cu^{2+} ion is at a bond length of 2.99(1) Å from P. The various bond lengths and bond angles are given in Table III.

TABLE I. Cell parameters and refinement parameters after crystal structure refinement of BCTPO by FULLPROF.

Parameter	Value
Space group	$C12/c1$
Crystal system	Monoclinic
Lattice parameters	$a = 17.6634(2)$ Å, $b = 7.2850(1)$ Å, $c = 9.2103(1)$ Å, $\alpha = \gamma = 90^\circ$, $\beta = 100.029(1)^\circ$
Refinement parameters	$R_p = 14.1$, $R_{wp} = 14.3$, $R_{exp} = 10.29$, $\chi^2 = 1.94$

B. Magnetic measurements

The T-dependent magnetic susceptibility [$\chi(T) = M/H$, where $M(T)$ is the magnetization and H is the applied magnetic field] of BCTPO is shown in Fig. 3. $\chi(T)$ increases as the temperature decreases and shows a broad maximum around 53 K which is possibly due to short-range magnetic correlations in this coupled spin-chain system. On further lowering the temperature, $\chi(T)$ exhibits an upturn below 16 K and follows a Curie-like behavior down to 2 K. This is thought to be due to broken chains and/or paramagnetic impurities. Further, to explain $\chi(T)$ data quantitatively we model the

TABLE II. Atomic positions obtained after refinement of the XRD data at 300 K of BCTPO.

Atom	x	y	z	Occupancy
Ba	0.1457(01)	0.6312(04)	0.6087(03)	1
Te	0.0587(02)	0.8443(04)	−0.0693(04)	1
Cu1	0.0000	0.6934(11)	0.2500	0.5
Cu2	0.2500	0.7500	0.0000	0.5
P	0.1601(08)	0.8396(19)	0.2784(14)	1
O1	0.1070(14)	0.9459(29)	0.1461(26)	1
O2	0.2317(13)	0.7918(27)	0.2003(34)	1
O3	0.1974(13)	0.8987(36)	0.4326(27)	1
O4	0.1504(17)	0.7261(30)	−0.0958(33)	1
O5	0.1093(16)	0.6917(37)	0.2848(27)	1
O6	0.0000	0.7621(44)	−0.2500	0.5
O7	−0.0211(15)	0.7387(34)	0.0358(37)	1

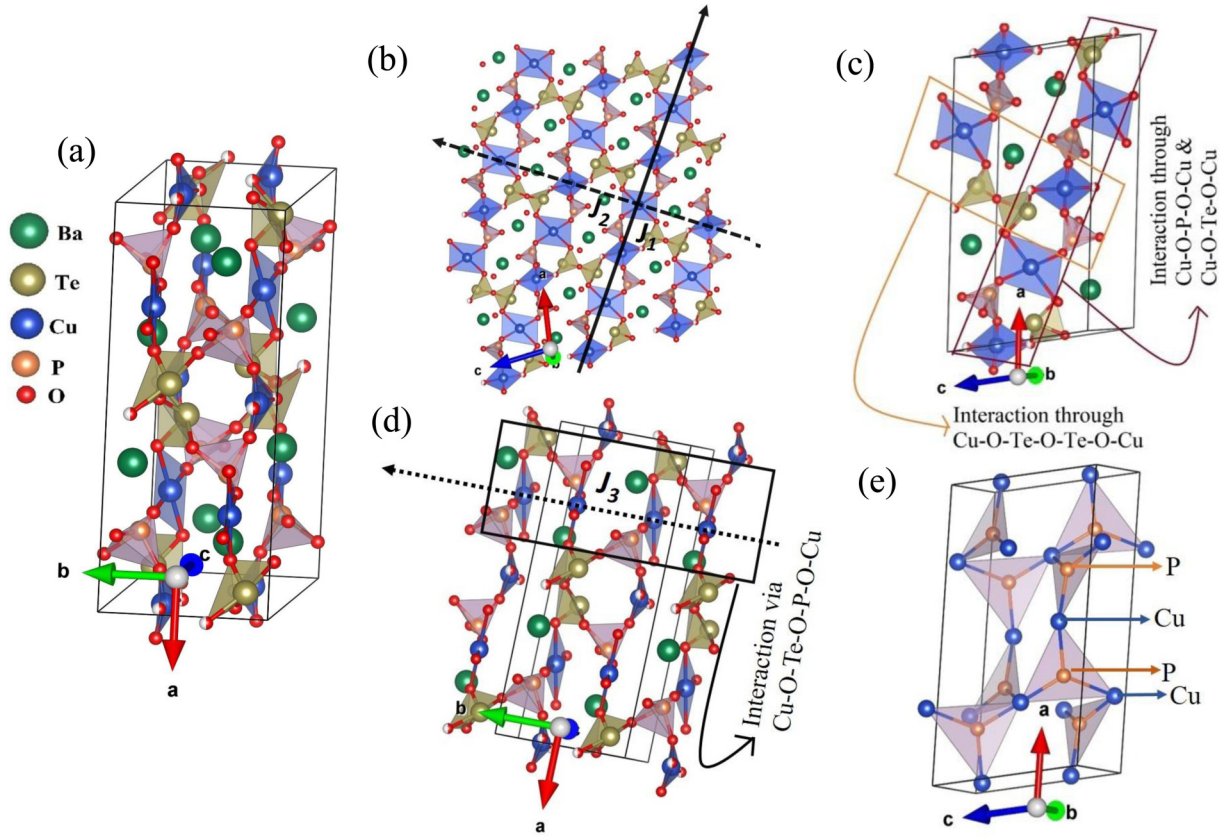

FIG. 2. The crystal structure of BCTPO is shown. (a) The unit cell of BCTPO. (b) Two-dimensional projection of the crystal structure of BCTPO in the *a*-*c* plane. The solid line shows the intrachain exchange interaction J_1, and the dashed line shows the interchain exchange interaction J_2. (c) Paths of intrachain and interchain interaction among Cu^{2+} ions in the *a*-*c* plane. (d) Interplanar interaction among Cu^{2+} ions in BCTPO by exchange coupling constant J_3 and its path. (e) Distribution of three Cu^{2+} ions around P in BCTPO.

susceptibility as follows:

$$\chi(T) = \chi_0 + C_p'/(T - \theta_p') + \chi_{\text{spin}}(T), \tag{1}$$

where χ_0 is the temperature-independent contribution to the susceptibility. C_p' is the Curie constant, and θ_p' is the Curie-Weiss temperature due to the extrinsic paramagnetic contribution in the sample. $\chi_{\text{spin}}(T)$ is the susceptibility of the uniform 1D HAF chain system with nearest-neighbor interaction (J/k_B). To fit our data we used Eq. (53) from Ref. [15]. For the fitting we have chosen the temperature range 2–400 K (see Fig. 3). Our attempts to describe the data with the dimer or the interacting-dimer model did not result in good fits.

Upon fitting, we obtained $J/k_B = 90$ K, which is close to the reported value in Ref. [13]. The T-independent susceptibility is $\chi_0 = (-5.4 \pm 0.4) \times 10^{-5}$ cm^3/mol Cu, which (after accounting for the core diamagnetic susceptibility) gives the Van Vleck susceptibility χ_{vv} to be 0.82×10^{-4} cm^3/mol Cu and the value of the Curie constant extracted from extrinsic contribution, $C_p' = (0.0137 \pm 0.0003)$ cm^3 K/mol Cu. We also obtained $g = 2.06$, which shows the presence of some spin-orbit coupling as observed in other copper systems also. We also note that in high fields (50 and 70 kOe), an anomaly is seen in the temperature derivative of the susceptibility $\frac{d\chi}{dT}$ at around 4 K (see the top inset in Fig. 3).

Further, to calculate θ_p' with better accuracy, we subtracted χ_0 and χ_{spin} from the total $\chi(T)$ data. Thereafter, taking the inverse of $C_p'/(T - \theta_p')$, we plot it as a function of T in the bottom inset in Fig. 3. As this extrinsic Curie-like contribution is prominent only at low temperatures, we have taken a T range of 2–5 K for a linear fit and extracted $\theta_p' \sim -1.3$ K.

Incidentally, considering the exchange constant $J/k_B = 90$ K from the 1D HAF chain model fitting and given the ordering observed around 4 K in $C_p(T)$ data in a field and in NMR data (see the following sections), a moderate frustration parameter, $|\ (J/k_B)/T_N\ | \sim 23$, is obtained for BCTPO.

TABLE III. Bond lengths and bond angles for the interaction paths Cu-O-P-O-Cu and Cu-O-Te-O-Te-O-Cu in the unit cell of BCTPO.

Bond length (Å)	Bond angle (deg)
Cu − O5 = 1.90(3), O5 − P = 1.41(4)	∠Cu − O5 − P = 129(2)
P − O2 = 1.59(3), O2 − Cu = 1.95(3)	∠O5 − P − O2 = 115.1(18)
Cu − O4 = 1.83(3), O4 − Te = 1.89(3)	∠P − O2 − Cu = 136.6(15)
Te − O6 = 1.898(10)	∠O7 − Cu − O5 = 79.7(12)

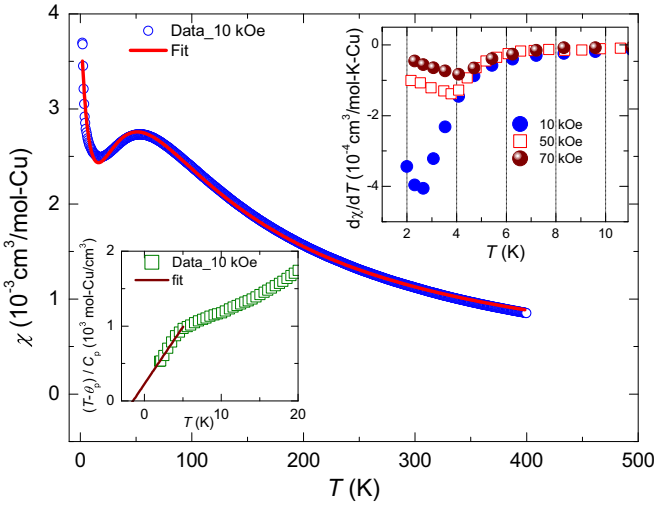

FIG. 3. The magnetic susceptibility $\chi(T)$ of BCTPO is shown as a function of temperature at 10 kOe, and the fitting is done by the 1D HAF chain model as explained in the text. Bottom inset: The inverse of the susceptibility due to extrinsic paramagnetic impurities is plotted as a function of T, and to extract θ_p, a linear fit in the T range of 2–5 K is shown. Top inset: $\frac{d\chi}{dT}$ is shown as a function of T in various applied fields.

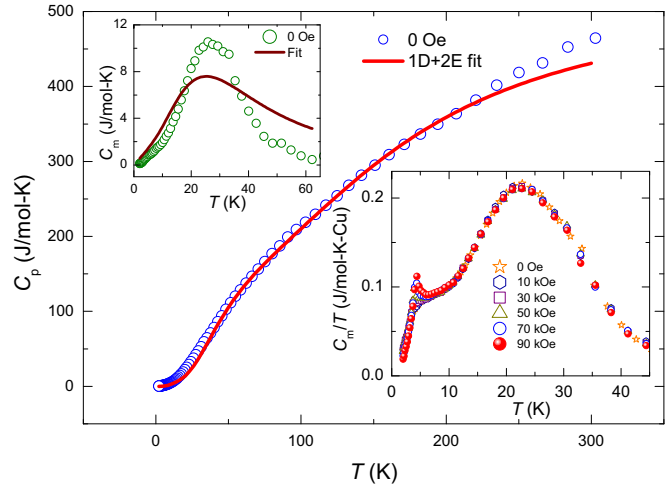

FIG. 4. The heat capacity $C_p(T)$ as a function of temperature in zero field together with a fit by a combination of one Debye and two Einstein terms (1D+2E) for BCTPO is shown. Top inset: The magnetic heat capacity C_m in zero field is shown along with a fit to the uniform HAF chain model (see text). Bottom inset: C_m/T as a function of T at different applied magnetic fields is shown.

C. Heat capacity

To check for any signatures of low dimensionality and LRO, we measured the heat capacity $C_p(T)$ as a function of temperature.

The total heat capacity of a magnetic insulator comprises heat capacity due to the lattice C_{lattice} and heat capacity due to the magnetic ions C_m [16]. So to extract C_m one has to subtract C_{lattice} from the total C_p. In the absence of a proper nonmagnetic analog for BCTPO we used a combination of Debye and Einstein terms [17] for the lattice heat capacity:

$$C_{\text{lattice}}(T) = C_{\text{Debye}} + C_{\text{Einstein}}, \tag{2}$$

where

$$C_{\text{Debye}} = C_D\left[9nR\left(\frac{T}{\theta_D}\right)^3\int_0^{\theta_D/T}\frac{x^4e^x}{(e^x-1)^2}dx\right], \quad x = \frac{h\omega}{k_BT},$$

and

$$C_{\text{Einstein}} = \sum C_{Ei}\left[3nR\left(\frac{\theta_{Ei}}{T}\right)^2\frac{e^{\left(\frac{\theta_{Ei}}{T}\right)}}{\left(e^{\left(\frac{\theta_{Ei}}{T}\right)}-1\right)^2}\right].$$

Here n is the number of atoms in a formula unit, C_D is the weight factor for the Debye term, C_{Ei} are weight factors for the Einstein terms, k_B is the Boltzmann constant, h is Planck's constant, ω is the angular frequency of vibration, θ_D is the Debye temperature, and θ_{Ei} are the Einstein temperatures. For fitting we have chosen the temperature range 90–200 K, which implicitly assumes that the magnetic contribution is negligible above 90 K.

In Fig. 4, $C_p(T)$ data in zero field are plotted as a function of temperature, and the fitting is done with a combination of one Debye and two Einstein terms. Taking $n = 21$, the parameters obtained from the fitting are $C_D = 0.048$, $\theta_D = 91$ K; $C_{E1} = 0.55$, $\theta_{E1} = 600$ K; and $C_{E2} = 0.39$, $\theta_{E2} = 170$ K. Here θ_D is relatively smaller than the reported value in Ref. [13] (197 K); however, the coincidence of the fit with the experimental data is better in our case. In the top inset in Fig. 4, C_m at 0 Oe is shown, which is extracted after deducting C_{lattice} from the $C_p(T)$ data. One might have expected a broad maximum around 50 K as in $\chi(T)$ data. However, due to the large lattice contribution at these temperatures, we have poor accuracy in extracting the magnetic contribution. On fitting the data using Eqs. (54a)– (54c) from Ref. [15], where the coupling constant J/k_B is the only parameter, we get J/k_B for BCTPO of about 53 K. However, a large difference is seen between the fit and the experimental data. Indeed, the relatively poor accuracy of the magnetic contribution and also a deviation from the isolated chain geometry due to nonzero J_2 and J_3 likely play a big role. In the bottom inset in Fig. 4, C_m/T as a function of T at different applied magnetic fields is shown. On decreasing the temperature C_m/T increases, and after a broad maximum is attained, C_m/T decreases further on lowering the temperature. Around 4 K, C_m/T shows a sharp peak which hardly has any shift with increasing field.

In Fig. 5, $C_m(T)$ is plotted as a function of T for different applied magnetic fields. The peak seems to get sharper with increasing magnetic field. The sharp peak (∼4 K) suggests some ordering. Sharpening of the heat capacity anomaly on increasing the field is suggestive of fluctuations in the ground state which are frozen out by the field. An anomaly was seen at about 4 K in high fields in $\frac{d\chi}{dT}$ as well. $C_m(T)$ follows a power law ($C_m \propto T^\beta$) behavior below the ordering temperature ($T_N \sim 4$ K). A power law fit is shown in the bottom inset in Fig. 5. The extracted values of the exponents are 2.5, 2.8, 3.1, and 3.3 for 0, 10, 50, and 90 kOe, respectively. The exponent values suggest antiferromagnetic magnon-phonon coupling [18] and three-dimensional ordering [19].

In the top inset in Fig. 5 we show the change in magnetic entropy ΔS_m by integrating C_m/T with respect to T. We

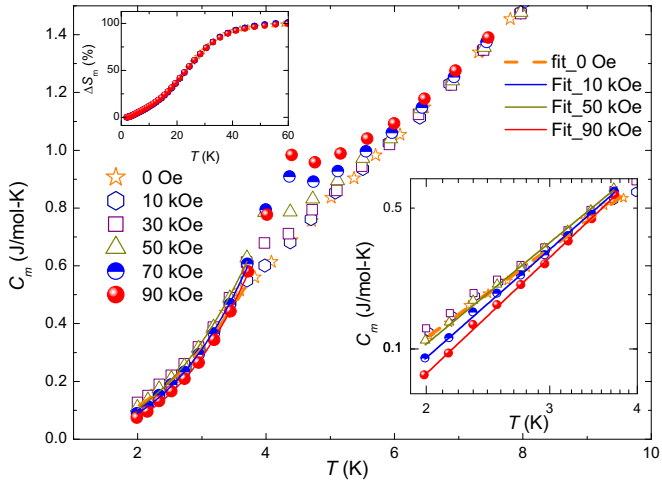

FIG. 5. Magnetic heat capacity $C_m(T)$ as a function of temperature for BCTPO at different applied magnetic fields is shown, and a power law (see text) fitting is done below the ordering temperature for different applied magnetic fields. Bottom inset: An enlarged view of the power law fits (log-log scale) is shown at various magnetic fields. Top inset: The change in magnetic entropy $\Delta S_m(T)$ as a function of T at different applied magnetic fields is plotted for BCTPO.

obtained $\Delta S_m \sim R\ln(2S+1)$, with $S = \frac{1}{2}$, which reflects that BCTPO is an ordered system. Note that most of the entropy is recovered well above the 4 K transition. This indicates that the field-induced order has a complex nature and that only a small fraction of the Cu moments might show the usual long-range order.

D. ^{31}P NMR

In BCTPO, ^{31}P appears to be a good nucleus to probe through NMR as it has 100% natural abundance with nuclear spin $I = \frac{1}{2}$. Here ^{31}P is coupled to Cu through O. So by measuring the ^{31}P spectra, shift, and spin-lattice relaxation rate $1/T_1$, we can study the static and dynamic properties associated with the magnetic Cu lattice in BCTPO. It is also noted that small amounts of extrinsic impurities which might strongly affect $\chi(T)$ at low temperatures do not impact the NMR measurements.

1. Spectra and NMR shift

In BCTPO there is only one ^{31}P site and two different Cu^{2+} ion sites. These two Cu^{2+} ions are coupled to ^{31}P via oxygen through a superexchange coupling. Also, the electrons of the magnetic ion Cu^{2+} impact the ^{31}P nuclei through a transferred hyperfine coupling A_{hf}. In Fig. 6, ^{31}P spectra for BCTPO at different temperatures are shown as a function of frequency ν, and the vertical dashed line shows the reference ^{31}P position at a magnetic field of 93.954 kOe (by taking H_3PO_3 to be the nonmagnetic reference). The spectral position at various temperatures shows a shift due to the hyperfine interaction with the magnetic Cu^{2+} ions. The spectral lines are asymmetric due to the anisotropy of the spin susceptibility and/or anisotropy of the hyperfine coupling. As shown in Fig. 6, the peak position of the spectrum shifts to higher frequencies on decreasing the temperature. It then shows a broad maximum around 54 K,

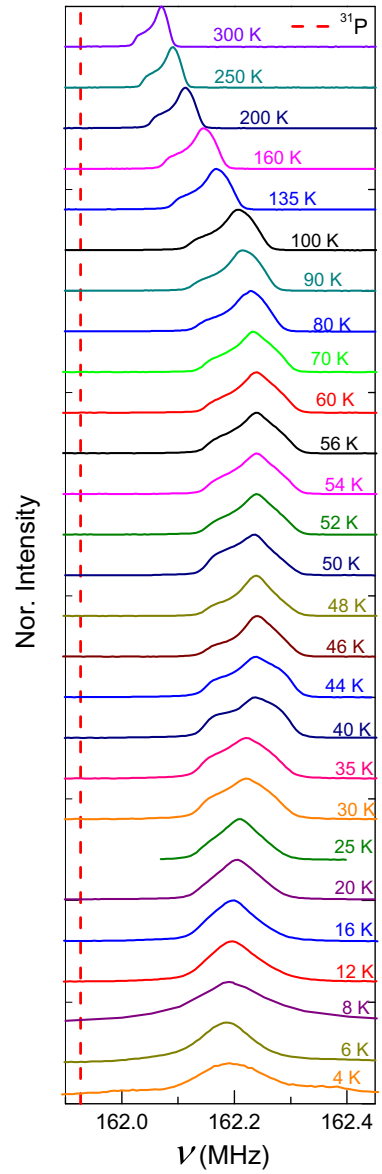

FIG. 6. The temperature-dependent ^{31}P NMR spectrum of BCTPO at a fixed magnetic field of 93.954 kOe is shown at different temperatures from 4 to 300 K. The reference position for ^{31}P is shown by a vertical dashed line.

after which it shifts to lower-frequency values. The broad maximum in the T-dependent spectral position suggests short-range correlations. The large broadening around 4 K is likely due to the onset of static magnetic order.

To estimate the ^{31}P NMR powder-averaged line shifts ($K_{\rm iso}$, $K_{\rm aniso}$, K_{ax}) from our experimentally taken spectra as a function of temperature, we simulated the line shapes at different temperatures and compared the results with the measured data.

Fixing $K_{\rm aniso} = 0$ and taking $K_{\rm iso}$ and K_{ax} to be variable parameters, we simulated the experimental spectra. In Fig. 7 the full width at half maximum (FWHM) of the spectra for BCTPO is shown as a function of T. As one can see, on lowering T, FWHM increases and shows a broad maximum

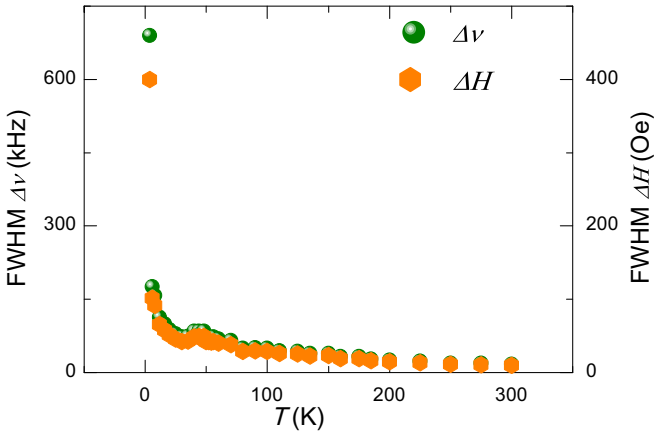

FIG. 7. The FWHM $\Delta\nu$ and the FWHM ΔH for the ^{31}P spectrum are plotted as a function of T on the left and right y axes, respectively, for BCTPO (in semilog scale).

or plateau at around 48 K which is due to short-range correlations. On further lowering the temperature it shows an upturn and diverges for $T \to 0$, which is typical near the onset of LRO. Taking $K_{\rm aniso} = 0$, $K_{\rm iso}$ provides the powder average intrinsic susceptibility. Our inferred $K_{\rm iso}(T)$ for BCTPO is shown as a function of temperature in Fig. 8 (left y axis). $K_{\rm iso}$ increases on lowering the temperature and shows a broad maximum at $T \sim 50$ K, as seen in the susceptibility data (see Fig. 3). On the right y axis of Fig. 8, $\chi(T)$ is shown as a function of temperature for BCTPO, which tracks $K_{\rm iso}(T)$. In Fig. 9 the axial NMR shift $K_{ax}(T)$ is seen to have similar variation.

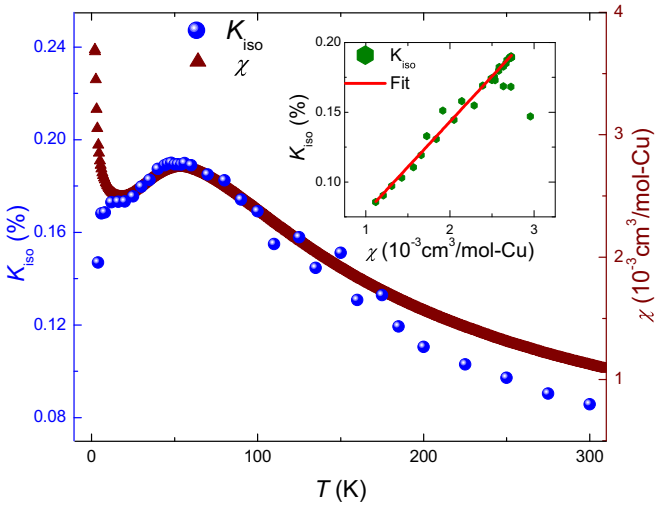

FIG. 8. The right y axis shows the susceptibility as a function of temperature. The left y axis shows the temperature-dependent isotropic ^{31}P NMR shift as a function of temperature. Inset: The variation of the isotropic ^{31}P NMR shift is shown as a function of the magnetic susceptibility $\chi(T)$ by taking the temperature to be implicit parameter, and its linear fit is shown by the solid line.

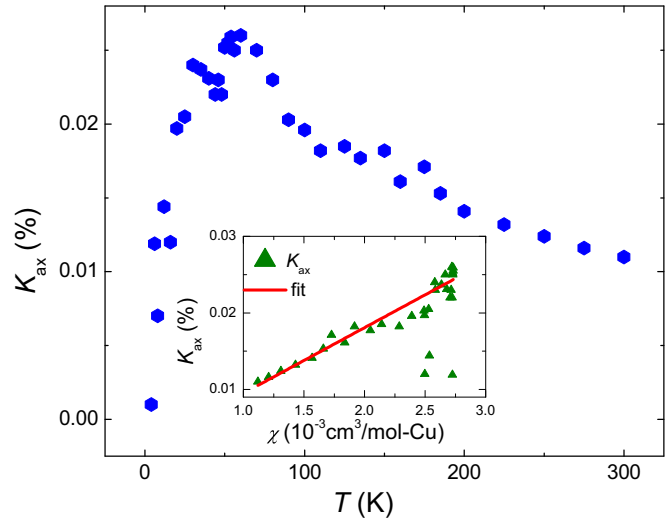

FIG. 9. Axial ^{31}P NMR shift $K_{ax}(T)$ for BCTPO is shown as a function of temperature. It shows a broad maximum around 50 K. Inset: $K_{ax}(T)$ is plotted as a function of $\chi(T)$ with temperature being an implicit parameter, and the solid line is a linear fit to the data.

The NMR shift $K(T)$ directly reflects spin susceptibility $\chi_{\rm spin}(T)$, so one can write

$$K(T) = K_0 + \frac{A_{hf}}{N_A \mu_B}\chi_{\rm spin}, \tag{3}$$

where K_0 is the temperature-independent chemical shift, A_{hf} is the total hyperfine coupling constant, N_A is Avogadro's number, and μ_B is the Bohr magneton. In the inset in Fig. 8, $K_{\rm iso}$ is plotted as a function of χ, taking T to be an implicit parameter. The linear fit gives the isotropic-hyperfine coupling constant $A_{hf}^{\rm iso} \simeq 3539$ Oe/μ_B. To estimate the value of the axial-hyperfine coupling constant A_{hf}^{ax}, K_{ax} is plotted as a function of χ, taking T to be an implicit parameter in the inset in Fig. 9. The extracted $A_{hf}^{ax} \simeq 479$ Oe/μ_B. From the linewidth $\Delta\nu$ one could estimate the average local field at the ^{31}P site ($\Delta H = \frac{2\pi\Delta\nu}{\gamma}$, γ is the gyromagnetic ratio; see Fig. 7) to be about 400 Oe at 4 K. Taking $A_{hf}^{\rm iso} \sim 3539$ Oe/μ_B suggests an ordered moment of only $\sim 0.1\mu_B$. This is more evidence of the unconventional nature of the field-induced order.

2. *Spin-lattice relaxation rate* $1/T_1$

The temperature-dependent spin-lattice relaxation rate $1/T_1$ is shown in Fig. 10 for BCTPO. We used the saturation recovery method for the measurements. In the inset in Fig. 10 the recovery of the longitudinal nuclear magnetization m as a function of time delay t_d is shown for some selected temperatures. We used a single exponential fit for the recovery of the longitudinal nuclear magnetization of ^{31}P, as is expected for $I = \frac{1}{2}$ nuclei. At our lowest temperatures the data deviate from the single exponential function, perhaps due to the onset of static magnetism.

From Fig. 10 one can see that $1/T_1$ decreases on lowering the temperature down to 17 K, and further, it shows a sharp increase down to 4 K which we hypothesize is due to the onset of LRO (at or below 4 K) as a result of interchain interactions.

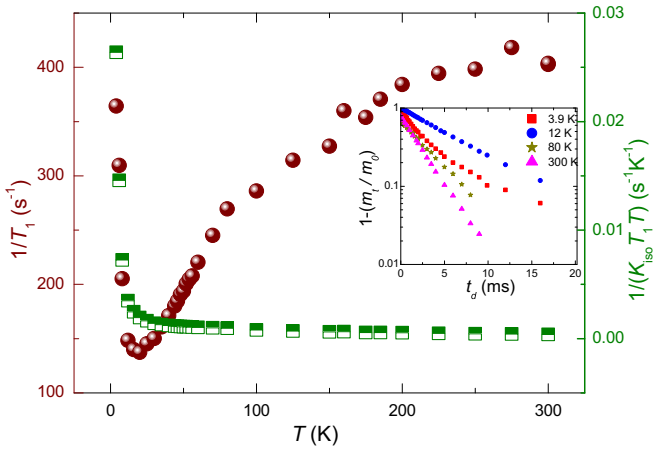

FIG. 10. On the left y axis the spin-lattice relaxation rate $1/T_1$ is plotted, and on the right y axis $1/(K_{\rm iso}T_1T)$ is plotted as a function of temperature. Inset: The recovery of the longitudinal nuclear magnetization of ^{31}P as a function of time delays t_d is presented in semilog scale for some selected temperatures. Here m_t is magnetization at time delay t_d, and m_0 is the saturation magnetization.

The contribution of the local moment to the spin-lattice relaxation rate $1/T_1$ is given by [20,21]

$$\frac{1}{T_1} = \frac{2k_BT}{\hbar^2}\left(\frac{\gamma_n}{\gamma_e}\right)^2 A_{hf}^2 \Sigma_{\mathbf{q}}[\chi''(\mathbf{q},\omega)/\omega], \tag{4}$$

where the sum is over the wave vectors $\mathbf{q}$. γ_n and γ_e are the nuclear and electronic gyromagnetic ratios, respectively. A_{hf} is the hyperfine coupling constant independent of $\mathbf{q}$, and $\chi''(\mathbf{q},\omega)$ is the $\mathbf{q}$-dependent imaginary part of the dynamical susceptibility at the nuclear Larmor frequency ω; the summation is over all wave vectors. In the limit $\omega \longrightarrow 0$ the summation takes the form $\frac{\chi^{\rm loc}(T)}{\omega_e}$, where $\chi^{\rm loc}(T)$ is the static local moment susceptibility per mole of magnetic ion and ω_e is the electron fluctuation frequency. Consequently, one expects $1/K_{\rm iso}T_1T$ to be independent of temperature. This is shown in Fig. 10 (right y axis), where the constancy appears to be valid at high T. A deviation might be expected anyway as one approaches the short-range ordering temperature of about 50 K.

In the high-temperature limit the susceptibility is Curie-like (C/T), and the relaxation rate becomes T independent and can be written as $\frac{1}{T_1} = 3\frac{2k_BT}{\hbar^2}(\frac{\gamma_n}{\gamma_e})^2 A_{hf}^2 \frac{C}{N_A\omega_e}$, where the electron fluctuation frequency is $\omega_e = \frac{J}{\hbar}\sqrt{\frac{8zS(S+1)}{3}} \simeq 2.78 \times 10^{13}$ rad/s, where we assume uncorrelated fluctuations of three Cu neighbors of ^{31}P. Here z is the number of nearest-neighbor Cu atoms for each Cu, which is 3 in the case of BCTPO. The exchange coupling J/k_B is found (in the mean-field approach) to be about 90 K from a fit to the 1D HAF chain model. Taking the hyperfine field value per Cu to be $\frac{1}{3}A_{hf}^{\rm iso} = \frac{1}{3} \times 3635$ Oe/$\mu_{\rm B}$, we evaluate $1/T_1 \simeq 9$ s^{-1}. This value is around two orders of magnitude smaller than the experimentally measured relaxation rate of about 400 s^{-1}. The difference evidences strong correlations among the spins which explain the strong frustration and the absence of order in the first place.

IV. CONCLUSIONS

We prepared single-phase polycrystalline $Ba_2Cu_2Te_2P_2O_{13}$ and analyzed its structural and magnetic properties through various experimental techniques like powder XRD, $\chi(T)$, $C_p(T)$, and NMR. XRD measurement showed that BCTPO is a single-phase sample with the monoclinic space group $C12/c1$. Structural data suggest the formation of coupled Cu^{2+} chains. Magnetization measurements do exhibit a broad maximum at around 53 K due to intrachain interaction among Cu^{2+} ions. A fit of $\chi(T)$ data to the $S = \frac{1}{2}$ 1D HAF chain model (see Ref. [15]) yields $J/k_B \sim 90$ K. However, our inferred magnetic heat capacity is not well fitted by the $S = \frac{1}{2}$ 1D HAF chain model, which is likely a result of interchain interactions. Further, the magnetic entropy change ΔS_m is ~5.75 J/mol K [close to $R\ln(2S+1)$ for $S = \frac{1}{2}$], and most of the entropy decrease (~95%) has already taken place before the system reaches some form of field-induced LRO at $T \sim 4$ K. NMR shift analysis shows short-range fluctuations around 54 K. Analysis of asymmetric NMR spectra based on hyperfine coupling anisotropy shows isotropic and axial components of the hyperfine coupling constants are $A_{hf}^{\rm iso} \simeq 3539$ Oe/$\mu_{\rm B}$ and $A_{hf}^{ax} \simeq 479$ Oe/$\mu_{\rm B}$, respectively. The spin-lattice relaxation rate $1/T_1$ shows an upturn at low temperature which appears to be due to critical fluctuations on the verge of long-range order caused by interchain interactions. The NMR linewidth also shows a large increase at low T due to evolving local fields near LRO.

We saw clear evidence of LRO at $T \sim 4$ K in our heat capacity data which appears to have been missed in earlier measurements [13]. Our temperature-dependent magnetization data also show an anomaly at about 4 K in fields of 50 and 70 kOe. The sharpening of the heat capacity anomaly with a field suggests that an applied field promotes long-range magnetic order. While our NMR data give indications of an ordered state at low T, NMR measurements below 4 K would be useful to do establish the ordering temperature. Furthermore, it would be rather interesting to study BCTPO at much higher fields. Neutron diffraction in zero field or muon spectroscopy would help one to check if the ground state has a true LRO. Additionally, *ab initio* calculations would be helpful to understand the relative importance of various exchange paths in this system.

ACKNOWLEDGMENTS

We acknowledge the financial help and central facilities provided by IIT Bombay and IRCC. V.K. would like to acknowledge fruitful discussion with Dr. K. Rao Bommisetti.

[1] E. Lieb, T. Schultz, and D. Mattis, Ann. Phys. (NY) **16**, 407 (1961).
[2] I. Affleck, J. Phys.: Condens. Matter **1**, 3047 (1989).
[3] N. D. Mermin and H. Wagner, Phys. Rev. Lett. **17**, 1133 (1966).
[4] H. Bethe, Z. Phys. **71**, 205 (1931).

[5] N. Motoyama, H. Eisaki, and S. Uchida, Phys. Rev. Lett. **76**, 3212 (1996).
[6] S. Eggert, I. Affleck, and M. Takahashi, Phys. Rev. Lett. **73**, 332 (1994).
[7] F. D. M. Haldane, Phys. Rev. B **25**, 4925 (1982).
[8] T. Tonegawa and I. Harada, J. Phys. Soc. Jpn. **56**, 2153 (1987).
[9] Y. Sasago, N. Koide, K. Uchinokura, M. C. Martin, M. Hase, K. Hirota, and G. Shirane, Phys. Rev. B **54**, R6835 (1996).
[10] H. Fukuyama, T. Tanimoto, and M. Saito, J. Phys. Soc. Jpn. **65**, 1182 (1996).
[11] E. Dagotto, J. Riera, and D. Scalapino, Phys. Rev. B **45**, 5744 (1992).
[12] A. Vasiliev, O. Volkova, E. Zvereva, and M. Markina, npj Quantum Mater. **3**, 18 (2018).
[13] M. Xia, S. Shen, J. Lu, Y. Sun, and R. Li, J. Solid State Chem. **230**, 75 (2015).
[14] J. Rodríguez-Carvajal (unpublished).
[15] D. C. Johnston, R. K. Kremer, M. Troyer, X. Wang, A. Klümper, S. L. Bud'ko, A. F. Panchula, and P. C. Canfield, Phys. Rev. B **61**, 9558 (2000).
[16] E. S. R. Gopal, *Specific Heats at Low Temperatures* (Springer, Berlin, 2012).
[17] N. Ashcroft and N. Mermin, *Solid State Physics*, HRW International Editions (Holt, Rinehart and Winston, New York, 1976).
[18] P. Pincus and J. Winter, Phys. Rev. Lett. **7**, 269 (1961).
[19] S. Joshua, Phys. A (Amsterdam, Neth.) **261**, 135 (1998).
[20] T. Moriya, Prog. Theor. Phys. **16**, 641 (1956).
[21] T. Moriya, J. Phys. Soc. Jpn. **18**, 516 (1963).